电 化 学
J. Electrochem. 2022, 28(3), 2108491 (1 of 20)

[Review] DOI: 10.13208/j.electrochem.210849 Http://electrochem.xmu.edu. cn

Recent Advances in Electrical Transport Spectroscopy for the *in Situ* Measurement of Electrochemical Interfaces

Zhang-Yan Mu, Meng-Ning Ding*

(*Key Laboratory of Mesoscopic Chemistry, School of Chemistry and Chemical Engineering, Nanjing University, Nanjing 210023, Jiangsu, China*)

Abstract: Electrochemical/electrocatalytic technology has played a central role in achieving highly efficient energy conversion and storage. To date, the in-depth electrochemical research begins to require accurate and multi-dimensional information of electrochemical interfaces, which usually relies on the application of *in situ* characterizations. Electrical transport spectroscopy (ETS) is a newly developed measurement strategy based on chip-platform, and provides *in situ* information of electrochemical interfaces from a novel perspective due to a signal origin that is fundamentally different from typical spectroscopic and electrochemical techniques. In this tutorial review, the working principle and experimental setup of ETS are described in detail with the demonstration of several model electrocatalytic materials, including metal nanoparticle/nanowires, two-dimensional layered materials, nickel based hydroxide/oxyhydroxides and dissimilatory metal-reducing bacteria. The advantages of ETS are summarized, and the future challenges and opportunities that ETS faces are also prospected.

Key words: electrical transport spectroscopy; mirco-nano electrochemical device; *in-situ* characterization; electrochemical interfaces; surface adsorptions

1 Introduction

Efficient conversion and storage of electric energy through electrochemical/electrocatalytic devices provide viable solutions towards a sustainable future. To keep advancing and optimizing the corresponding technologies and especially the catalyst efficiency, precise monitoring and in-depth understanding of the electrochemical interfaces is of critical value. However, such an electrochemical interface is always buried between a liquid electrolyte and a solid substrate (sometimes with gaseous reactants/products involved, see Figure 1 for the structure of a so-called electrochemical "double layer model"), and the intermediate states of electrodes during active electrochemical reactions only exist with applied working potentials, making it difficult to be accessed by *ex situ* characterization techniques. In this regard, *in situ* electrochemical spectroscopy, such as Raman, X-ray absorption spectroscopy (XAS), infrared (IR) spectroscopy, etc[1-5]. have been extensively developed over the past century, with tremendous success in the fundamental investigations on the electrochemical processes. However, due to the possible interference between the liquid layer and the incoming and/or outgoing electromagnetic waveforms (that is the general probe in the spectroscopic-based characterizations), *in situ* spectroscopic characterization of electrochemical interfaces usually requires specific thin-layer cells, synchrotron resources, or highly specialized probes or device designs to ensure high precision and

Cite as: Mu Z Y, Ding M N. Recent advances in electrical transport spectroscopy for the *in situ* measurement of electrochemical interfaces. *J. Electrochem.*, 2022, 28(3): 2108491.

Received: 2021-11-01, Revised: 2021-12-31. *Corresponding author, Tel: (86-25)89681724, E-mail: mding@nju.edu.cn

accuracy. Additionally, *in situ* characterization approaches based on other signaling strategies have also been reported, including scanning probe microscopy[6-7] and electrochemical impedance spectroscopy[8-9], yet each with own limitations. Overall, due to the extreme difficulty to obtain precise and quantitative *in situ* information from one single characterization method, it is always of great significance to develop novel *in situ* characterization technique and methodology, presumably equipped with distinct principles of signal generation, to help provide complementary insights from different aspects.

In 2015, Ding et al. developed an electrical transport spectroscopy (ETS) based on the design and utilization of a four-electrode micro-nano electrocatalytic device (containing an equivalent on-chip electrochemical cell), which has been quickly extended to different material systems and catalytic applications in the past several years[10]. Based on the principle of surface electron scattering that is especially sensitive to the surface adsorption states of metallic nanostructures, ETS was first employed to measure the adsorbates on metal catalyst surfaces during electrochemical processes. Later, ETS was demonstrated to enable the *in situ* monitoring electronic properties of electrode materials in a more general sense, which is sensitive to processes such as charge modulation, phase change, and etc. Overall, as ETS provides information with a different electrical transport-based signal source, coupling with on-chip cyclic voltammetry (CV), it can realize the *in situ* measurement of the varying interfacial states of broad range electrode materials, with significant advantages in sensitivity, specificity, and quantification, providing experimental basis for the fundamental study of electrochemical mechanisms under operando conditions. In this tutorial review, the advances of ETS will be introduced and discussed from views of adsorptions on metals, phase change and charge modulation on two-dimensional (2D) semiconductors and hydroxide/oxyhydroxides, and conducting mechanism of dissimilatory metal-reducing bacteria. We will focus on how to identify electrical transport signals, and how these signals can be used for the understanding and optimization of electrochemical interfaces. Finally, we summarize the remaining key issues and future opportunities of ETS correlated on-chip electrochemical platform.

2 Working Principle and Device Fabrication

The diffusive surface scattering of conducting electrons on the metal surface, which originates from the inelastic collision between the moving electrons and the surface atoms, is a well-established effect that causes loss of energy of the conducting electrons and therefore leading to reduced conductivity in metals. Note that this effect becomes more obvious with the reducing dimension (increased surface to bulk ratio) of metal structures, e.g., physical measurements revealed that the surface scattering plays a more critical role in the conductivity of metal nanowires. For the similar reason, additionally introduced adsorbates (ions, molecules, etc.) on metals can further act as electron scattering centers, most times bring up stronger Columbus interactions with electrons in metal, adding high values to applications such as gas sensing[11-12].

In general, the surface scattering induced resistance change in one-dimensional metallic nanowires can be calculated using the same equations that are used to describe the size dependence of metals[10, 13]:

$$\rho = \rho_0 \left(1+\frac{3}{4}(1-p)\right)\frac{\lambda}{d} \quad (d \gg \lambda) \tag{1}$$

$$\rho = \rho_0 \left(\frac{1-p}{1+p}(1-p)\times\frac{\lambda}{d}\right) \quad (d \ll \lambda) \tag{2}$$

where ρ is the resistivity of metallic wire, ρ_0 is the resistivity of bulk metal, λ is the corresponding electron mean free path, d is the wire diameter and p is the portion of conduction electrons specularly reflected on the metal surface (in contrast to diffusive reflection). The surface adsorbates cause additional diffusive scattering, and thus, the reduced p value and increased resistivity (ρ). Different metals have their specific λ, and when the diameter of nanomaterial is reduced, especially close to λ, the resistance change due to adsorption and electron scattering would be more significant (Figure 1(A)).

As shown in Figure 1(B), a double layer structure is formed at an electrode/electrolyte interface, with electrode surface atomic layers, inner Helmholtz plane (IHP), and outer Helmholtz plane (OHP). During an active CV scan (or any other methodology that controls/alters the electrochemical potential of the electrode materials), the adsorbates on the electrode surface change gradually with the sweeping working potential (Figure 1(B)), and the adsorbates (especially in IHP) would affect surface electron scattering and thus the resistivity of electrodes. Based on this phenomenon, Ding et al. combined the concept and common set-up of nano-electronic devices and electrochemical cells, and firstly designed an integrated, four-electrode micro-nano on-chip electrochemical cell/device out of platinum nanowire (PtNW) (Figure 2)[10]. By coupling the traditional three-electrode potentiostat system with the channel of electrical transport measurement, CV and ETs signals could be obtained simultaneously, enabling the control and sensitive detection of adsorption features on metal surfaces.

For a typical device fabrication process, Si wafer with top thermal oxide layer (typically 300 nm) and pre-patterned Au electrodes was used as a substrate. A poly(methyl methacrylate) (PMMA) film was spin-coated on the Si wafer. E-beam lithography (EBL) was then used to open windows with defined shape for the consequent thin film preparation. Pre-prepared (by co-solvent evaporation) free standing film of nanomaterials (catalysts) on a water surface was then transferred onto the substrate surface. After the removal of PMMA template layer, catalyst materials were then deposited on the device substrate with desired pattern designs. To eliminate the influence of electrolyte and to avoid electrochemical reactions on the metal electrodes, another layer of PMMA (which is electrochemmically inert) was then deposited on the device with spin-coating. A smaller window that only exposes nanowires was then opened by EBL to define an electrochemical window. The device, with the exposed nanowires and PMMA protected electrodes, was used for on-chip electrochemistry and *in situ* electrical transport spectroscopy.

A two-channel source-measure units (SMUs) system was used for ETS measurements, as illustrated in Figure 2. The first SMU channel functioned as a potentiostat (using four-wire configuration) to perform the on-chip CV by applying the potential (V_G) of source/drain electrode (acting as the working electrode, WE) as to the reference electrode (RE), while collecting the current (I_G) through the counter electrode (CE). The second SMU channel was used to record ETS signals by supplying a small bias potential (typically 50 mV or

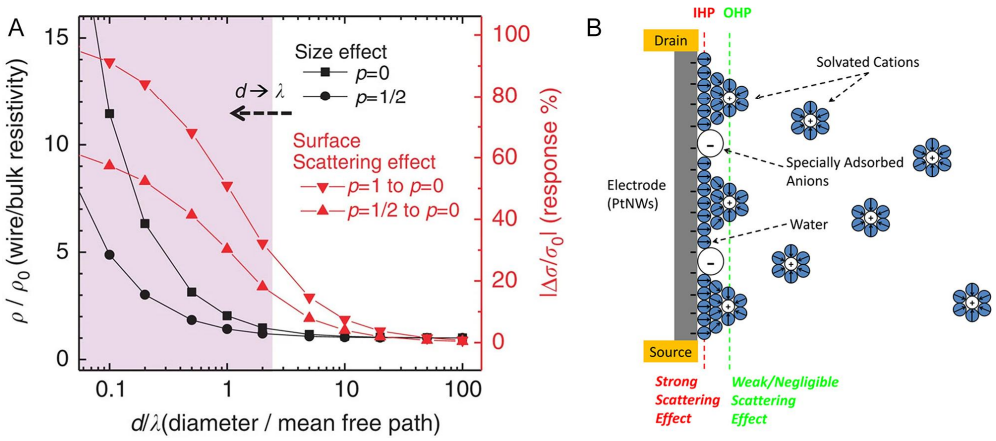

Figure 1 (A) Theoretical size and surface scattering effect of one-dimensional metallic wires. Black squares and circles represent the size dependent resistivity. Triangles represent the size dependent ETS responses caused by different electron scattering. (B) Schematic illustration of the double layer model in concurrent CV and ETS measurements. Reproduced with permission[10]. Copyright 2015, Nature Publishing Group. (color on line)

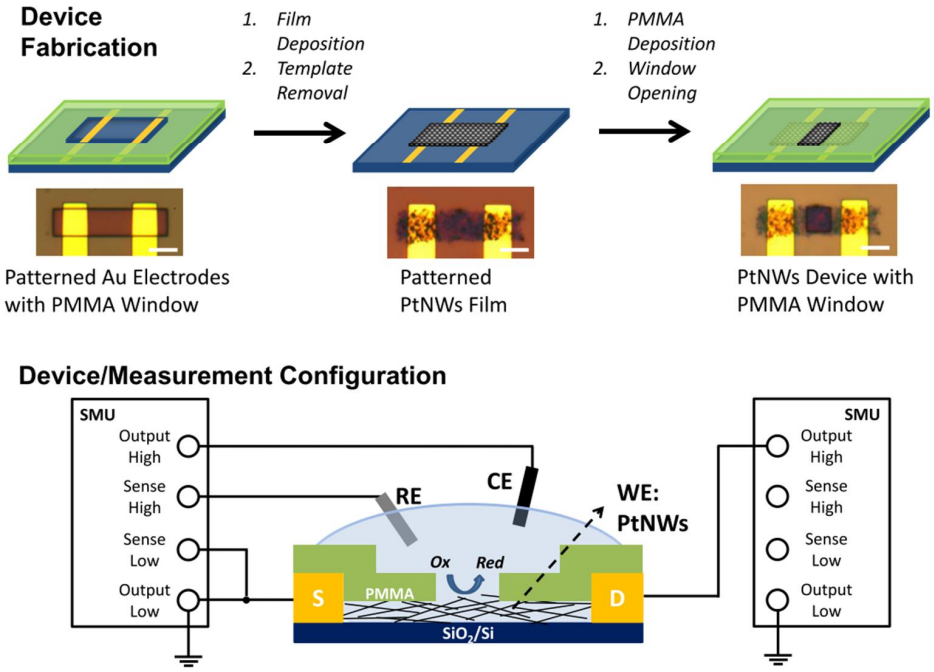

Figure 2 Schematic illustration and optical images of device fabrication process for concurrent CV and ETS measurements (top), and schematic illustration of the cross-sectional view of the device and the measurement configuration (bottom). Reproduced with permission[10]. Copyright 2015, Nature Publishing Group. (color on line)

smaller) between the source and drain electrodes, and collecting the electrically conductive current (I_{SD}).

3 *In Situ* ETS Study of Adsorptions on Metals Based on Surface Electron Scattering

Due to the unique adsorption and catalytic properties of noble and transition metals, metallic nanomaterials have been widely applied in the field of electrocatalysis, and the identifications of their surface states during active electrocatalytic processes have been regarded as key for further improving catalytic performances. Several examples of *in-situ* ETS study concerning Pt-catalyzed redox reactions and competitive anion adsorptions on Pt and Au surfaces are introduced as following.

3.1 Surface Adsorptions on PtNWs during Several Typical Redox Processes

The first to be introduced is the typical CV and ETS results of polycrystalline Pt in acidic electrolytes that are generally relevant to Pt-catalyzed water splitting and other reactions with the involvement of surface adsorbed oxygen/hydrogen intermediates. Typical results are shown in Figure 3. The CV result (the black curve in Figure 3(A)) includes five regions: hydrogen evolution reaction (HER), H adsorption/desorption region (H_{upd}), double layer (D.L.) region, surface oxide formation/reduction region (O_{upd}), and oxygen evolution reaction (OER)[14-16]. On the basis of electrode surface states, the ETS curve (the red curve in Figure 3(A), in the form of normalized relative conductance change ($\Delta G_{SD}/G_{SD}^0$)), can be correspondingly divided into three regions (marked by three colors in Figure 3(A)). The ETS signals corresponding to different adsorbates are generated following a diffusive scattering effect sequence: Pt-H < Pt-H_2O < Pt-OH < Pt-O. It is remarkable that G_{SD} exhibits a continuous decrease during OER, suggesting that the surface oxide formation does not reach the maximum coverage at the onset of OER, which is in contrast to a relatively complete and stable monolayer of adsorbed H(H_{ads}) atoms during HER process indicated by the flat G_{SD} character. To better visualize and analyze the ETS (G_{SD}) data, a differentiation operation can be applied to obtain the differentiated ETS

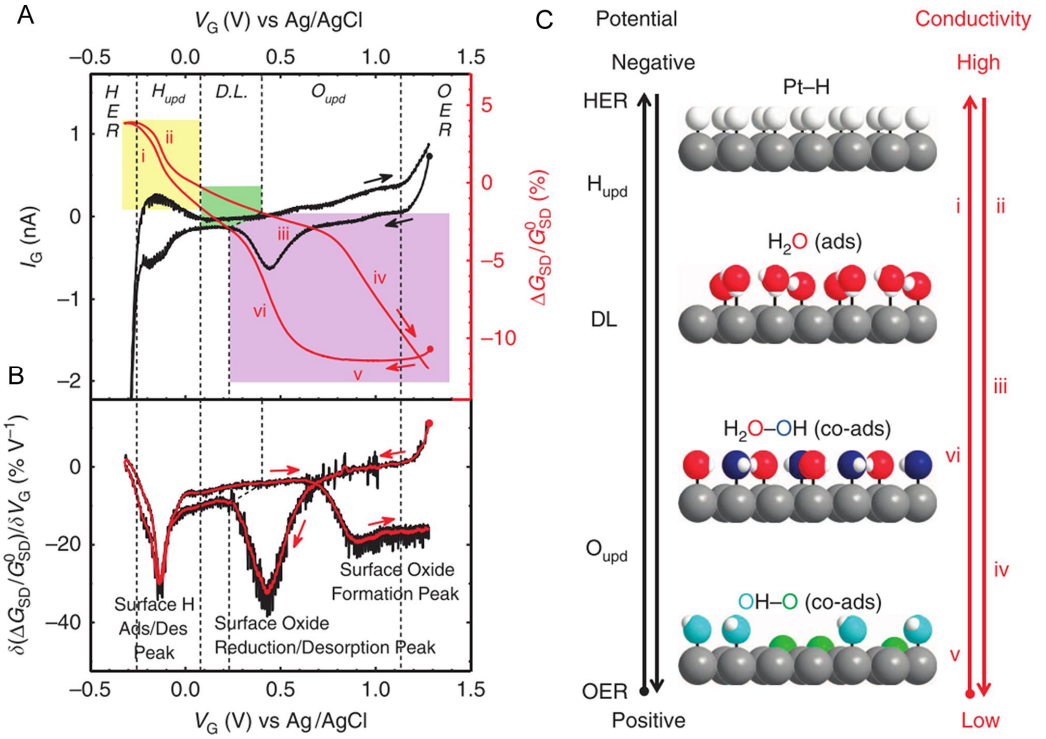

Figure 3 Electrical transport spectroscopic (ETS) measurement on the PtNWs in acidic condition. (A) I_G-V_G (CV) and G_{SD}-V_G (ETS) curves of PtNWs in 0.1 mol·L^{-1} $HClO_4$. (B) Differentiated result of ETS in (A) (dETS). (C) Schematic illustrations of the different surface states of Pt with the potential scanning (the left black axis) and the corresponding conductivity changes (the right red axis). Reproduced with permission[10]. Copyright 2015, Nature Publishing Group. (color on line)

(dETS) curve ($\delta(\Delta G_{SD}/G_{SD}^0)/\delta V_G$) (Figure 3(B)). Each change of surface states on the Pt electrode can be identified as a peak on the differentiation curve, which facilitates the sensitive detection of small conductivity changes caused by the adsorbates.

Since the perchlorate ion has been considered as one of the weakest adsorbed anions on Pt surface, the CV and ETS results of Pt in 0.1 mol·L^{-1} $HClO_4$ will serve as the baseline for further investigation of other electrocatalytic reactions (hydrogen peroxide reduction (PROR), methanol oxidation reaction (MOR) and formic acid oxidation reaction (FAOR)). These reactions are the most extensively studied model reactions for the understanding and developing of fuel cell technologies[17-20].

Figures 4(A) and 4(B) depict the on-chip CV and ETS results of polycrystalline Pt in 0.1 mol·L^{-1} $HClO_4$ with different concentrations of H_2O_2. With the increase of H_2O_2 concentration, large PROR redox currents dominate the voltammogram and cover up the intrinsic CV characteristics of PtNWs. The ETS results, with different signal sources (electrical transport) compared to the electrochemically based signals, are fundamentally not linked (and will not be affected) to the electrocatalytic redox current in the CV background. At a high concentration of H_2O_2, the G_{SD} curve drops to a lower value in the positive potential region and rises to a higher value in the negative range (Figure 4(B)), which suggest a larger percentage of the oxidized Pt surface and a larger coverage of H_{ads}, respectively. For a more detailed understanding of electrocatalysis, quantitative information of the electrode surface is often crucial. The drop of G_{SD} values with ascending amount of H_2O_2 can be observed at a given anodic potential, and this trend can be used to quantitatively estimate the surface coverage of O species (Figure 4(C)).

3.2 Intermediate Adsorptions on PtNWs during C1 Oxidations

For Pt-catalyzed MOR and FAOR, ETS can be

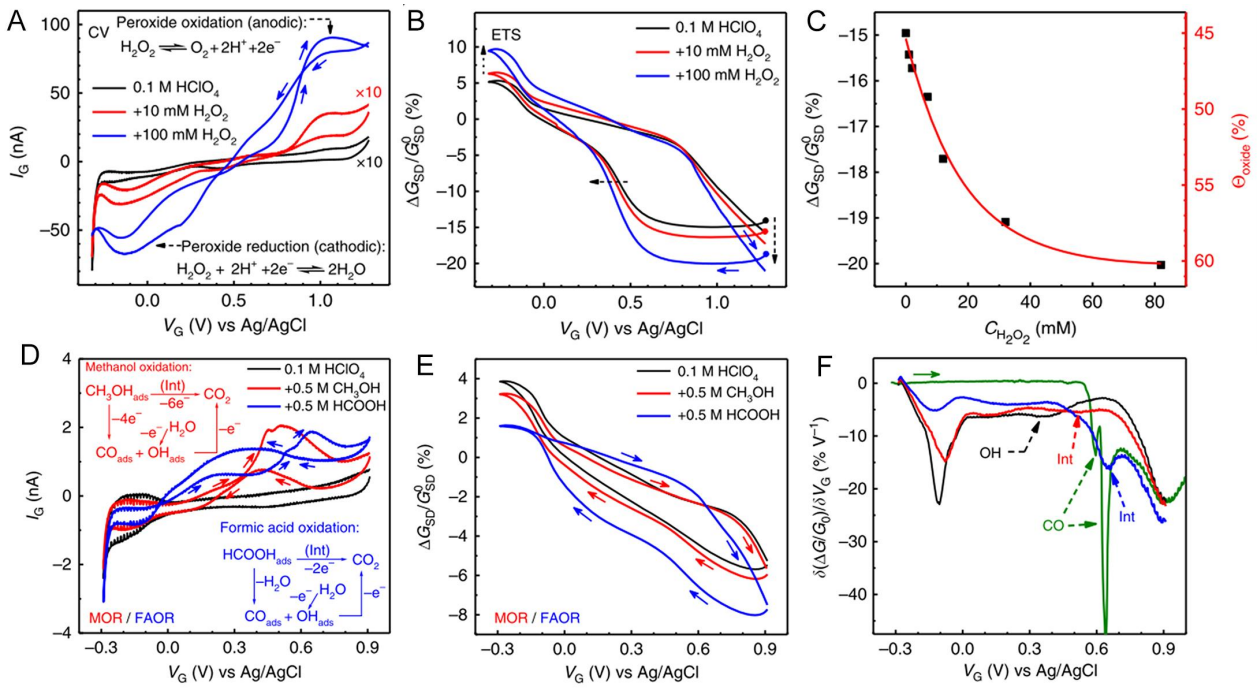

Figure 4 *In situ* ETS studies of PROR, MOR and FAOR on PtNWs. (A and B) I_G-V_G (CV) (A) and G_{SD}-V_G (ETS) (B) curves of Pt-NWs during PROR at different concentrations of H_2O_2 with the baseline process in $HClO_4$ (the black curve). (C) G_{SD} values (the black square) of the surface oxide at different concentrations of H_2O_2. (D and E) I_G-V_G (CV) (D) and G_{SD}-V_G (ETS) (E) curves of Pt-NWs during MOR and FAOR with the baseline process in $HClO_4$ (the black curve). (F) dETS curves of PtNWs during MOR (red), FAOR (blue) and CO striping (green). Reproduced with permission[10]. Copyright 2015, Nature Publishing Group. (color on line)

used for the detection of CO_{ads} intermediate (Figure 4 (F)), which leads to a self-poisoning effect on the surface. In addition, FAOR is accompanied by more significant poison than MOR due to the nonoxidative dehydration of formic acid, indicated by the more obvious change of ETS even in H adsorption/desorption region and double layer region. The ETS results of PtNW-catalyzed MOR and FAOR thus offer complemental results as an alternative source to other *in situ* electrochemical spectroscopy, such as *in situ* IR spectroscopy.

From the above Pt-catalyzed reactions, ETS can be used for the identification and quantitative characterization of reaction intermediates. It is also worth noting that the signal principle of ETS is significantly different from conventional spectroscopic methods, and external radiation energy is not required, which allows ETS to offer new insight into electrochemical interfaces that is not readily available previously with other approaches. However, it is also to be mentioned that the electrical transport signal does not involve any direct chemical structure information of reaction intermediates, making it necessary to coupling with other *in situ* characterization methods to resolve certain specific scientific questions.

3.3 Competitive Anionic Chemisorptions as a Descriptor for ORR Kinetics on PtNWs

In addition to the reactive molecules and/or intermediates, the electrolyte components (anions, cations and water) often have weaker surface adsorption energies yet significant impacts on the electrocatalytic performances through their interactions or competitive adsorptions with the reactants[21-24]. It is difficult yet urgent to achieve the identification of key promoters and inhibitors of reactions. To this end, ETS has been employed to detect the surface adsorptions of perchlorate, sulfate and halide ions on polycrystalline Pt surface[25]. Benefiting from the high sensitivity of ETS, the detection limit of Cl^- adsorption can reach 10^{-9} mol·L^{-1} (Figure 5(D)). Correspondingly, due

to the strong adsorption and poison by Cl^-, the ORR activity of Pt/C, which is crucial to advancing the sustainable commercialization of fuel cell, shows a significant decay with the site blocking of O_{ads} by Cl_{ads} at a trace level (10^{-6} mol·L^{-1}). It is remarkable that there is no change of molecular dipole moment for halide ions adsorbed on metal surface, which makes it cannot be characterized by *in situ* IR spectroscopy, while ETS is not limited by this due to the different signal sources (surface electron scattering).

ETS has also been employed to study the competitive adsorptions between CN^- and Cl^-, and the CN_{ads}-modified Pt/C shows high resistance to poison of Cl^- during ORR correspondingly[25]. This approach was further extended to eliminate the poison effect of Cl^- with a high concentration of ClO_4^- (one of the weakest binding anions on Pt). The anionic competition significantly reduces the halide adsorption on the Pt sur

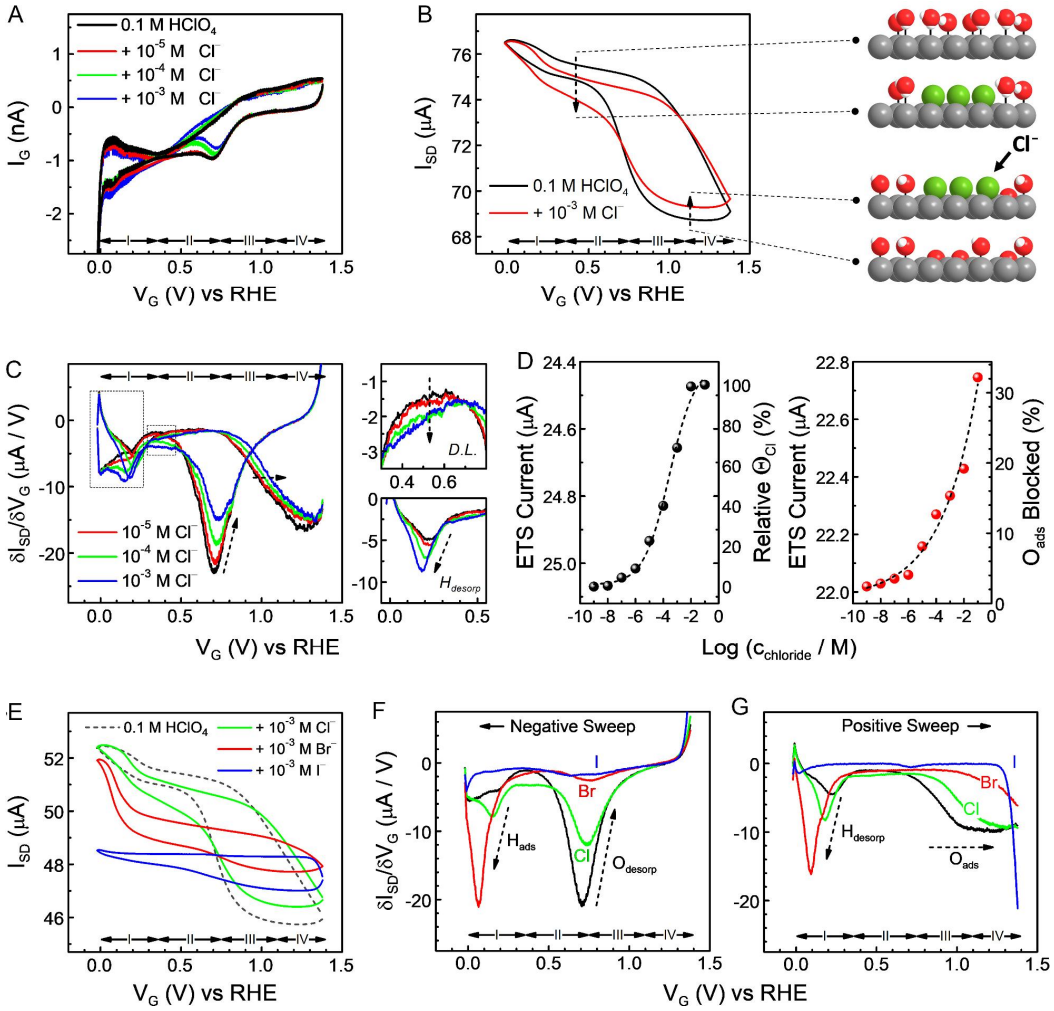

Figure 5 *In situ* ETS study of halide adsorption on Pt surface. (A) I_G-V_G (CV) curves of PtNWs in 0.1 mol·L^{-1} $HClO_4$ (black) and with the addition of varying concentrations of sodium chloride. (B) I_{SD}-V_G (ETS) curves of PtNWs in 0.1 mol·L^{-1} $HClO_4$ (black) and with the addition of 1 mmol·L^{-1} chloride anions (red). (C) dETS curves of PtNWs with varying chloride concentrations. Insets on the right depict the enlarged spectra at double layer and hydrogen desorption regions. (D) ETS current of the PtNWs device in D.L. (left, value obtained at 0.5 V vs. RHE) and oxidation (right, value obtained at 0.9 V vs. RHE) regions at different chloride concentrations. Electrically derived surface coverage of Cl_{ads} at the D.L. region and percentage of blocked O_{ads} by Cl_{ads} in oxidation region are given at the corresponding right axis. (E) I_{SD}-V_G (ETS) curves of PtNWs in 0.1 mol·L^{-1} $HClO_4$ and with the additions of 1 mmol·L^{-1} chloride, bromide and anions. (F, G) dETS characteristics of halide adsorptions. Reproduced with permission[25]. Copyright 2018, American Chemical Society. (color on line)

face, and this offers a promising solution, by simply optimizing the electrolyte content, to increase the impurity tolerance of fuel cell devices and their long-term durability.

Therefore, ETS signal is highly sensitive to ion adsorptions on metal surfaces, and the adsorption can be correlated with some electrocatalytic reaction processes based on the interactions of ions and interfacial reactants. Meanwhile, on the basis of ETS characterization results, the ionic environment can be further specifically designed to optimize the electrocatalytic system and promote the corresponding electrocatalytic performances.

3.4 "Weak Adsorbents" on Gold Nanoparticles

ETS measurement is theoretically a general approach for metallic materials with different compositions and morphologies, and this will benefit its application in more electrocatalytic reactions and catalyst developments. Mu et al. successfully fabricated micro-nano electrochemical devices out of platinum and gold nanoparticles (PtNPs and AuNPs) through self-assembly and obtained their ETS characteristics in acid-base conditions, which further provides the basis for the study of related electrocatalytic reactions (oxidations of CH_3OH, CO and etc.)[26]. In contrast to Pt, Au exhibits unique and significant perchlorate adsorption (presumably considered weak) under an acidic condition. As is shown in Figure 6(A), the I_{SD} of ETS decreases with the increase of ClO_4^- concentration, indicating more and stronger adsorptions of ClO_4^- on the Au surface. Weak adsorbates like ClO_4^- are hard to be characterized by cyclic voltammetry based on non-faradic current (in double layer region), whereas ETS signal has a relatively high sensitivity based on surface electron scattering. Moreover, a low scan rate of potential is beneficial to the accumulation of ions on electrodes (Figure 6(C-F)). Sulfate anion (SO_4^{2-}) is also regarded as a relatively weak adsorbate, but its adsorption is stronger than ClO_4^-, which also results in an inhibition in some electrocatalytic reactions[27]. Through the ETS study of Au, the adsorption difference of ClO_4^- and SO_4^{2-} can be obviously and systematically compared (Figure 6(G), (H)). It is obvious that ETS measurements can be potentially conducted on more metal-based nanomaterials, and this will facilitate its application in probing electrochemical interfaces during various electrochemical processes. Meanwhile, due to its high sensitivity, ETS can be potentially used for the detection of some widely considered weak adsorbates, including polyelectrolytes such Nafion.

4 The Phase Change and Charge Carrier Modulations Monitored by ETS

4.1 Electrochemical Intercalation of Two-Dimensional Materials

The integration of van der Waals (vdW) heterostructures brings unique properties and functions to two-dimensional layered materials (2DLMs)[28-29]. Electrochemical intercalation serves as an effective functionalization method for constructing superlattice structure with alternating monolayers of 2DLMs and intercalated ions[30,31]. The research of electrochemical intercalation mechanism and the optimization of intercalation also rely on the application of appropriate *in situ* characterization methods.

As is shown in Figure 7(A), ETS is conducted to monitor the conductivity change of MoS_2 during PTCDA intercalation, and the CV and ETS results can be divided into three regions (marked by different colors in Figure 7(A)). In Region I, conducting current I_{ds} increases gradually at relatively lower potentials until a steady state, resulting from the ionic-gating effect of the semiconducting MoS_2 channel via electrochemical double-layer, and the MoS_2 device shows a typical n-type semiconductor characteristic with an on/off ration of 106; In Region II, an obvious electrochemical (gate) current can be observed, representing the onset of an electrochemical transition; In Region III, the molecular intercalation (PTCDA) into vdW gaps of the MoS_2 nanosheet causes abrupt and stepwise increase of conductance after the onset potential of ~ -2.1 V vs. Ag/AgCl. Correspondingly, STEM-HAADF image reflects the uniformity and

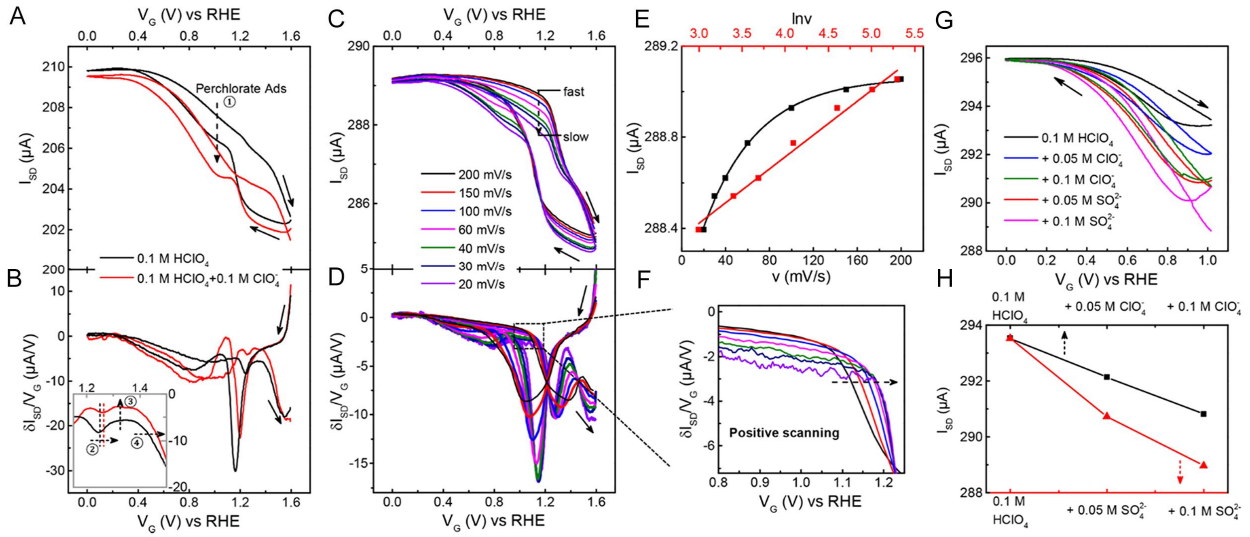

Figure 6 Perchlorate and sulfate adsorptions on AuNPs. (a and b) I_{SD}-V_G (ETS, (A)) and dETS (B) curves of AuNPs in 0.1 mol·L^{-1} $HClO_4$ (black) and with the addition of 0.1 mol·L^{-1} $NaClO_4$ (red). The inset shows the enlarged positive-going spectra of dETS curves in (B). (C and D) I_{SD}-V_G (ETS, (C)) and dETS (D) curves of AuNPs in 0.1 mol·L^{-1} $HClO_4$ with varying scan rates. (E) ETS current of AuNPs in the D.L. region (value from (C) obtained at 0.94 V) under different scan rates. (F) Enlarged positive-going spectra of dETS curves in (D). (G) I_{SD}-V_G (ETS) curves of AuNPs in 0.1 mol·L^{-1} $HClO_4$ with varying perchlorate and sulfate concentrations. (H) ETS current collected at 1 V in the positive-sweeping spectra of (G). Reproduced with permission[26]. Copyright 2020, American Chemical Society. (color on line)

interlayer spacing of the intercalated MoS_2 (Figure 7 (B)). The contraction of interl ayered PTCDA and MoS_2 will further change the electronic properties of MoS_2, which can be further used to reduce metal-MoS_2 contact barrier and lead to a molecular tunneling characteristic at the vertical direction[32].

4.2 Double Exchange Induced *in Situ* Conductivity Trend in Nickel Based Oxyhydroxides with Various Metal Doping

Nickel (Ni) based oxides and hydroxides materials have been widely used as non-noble metal OER catalysts because of their good catalytic performances in alkaline media[33]. The identification of active sites during catalysis will facilitate the preparation of the next generation of catalysts with high efficiency. Tian et al. detected the phase transition and *in situ* conductivity variations of Ni based oxyhydroxides by ETS during OER, establishing the correlation of intermediate resistivity, OER performance and electronic structure of a series of metal-doped Ni oxyhydroxide materials, and finally discovered new OER descriptor based on double exchange interaction[34].

As is shown in Figure 8, the initial conductivity (at about 1.3 ~ 1.4 V) of γ-NiOOH and α-$Ni(OH)_2$ are both low before Ni^{II}-Ni^{III} oxidation. The conductance of γ-NiOOH and α-$Ni(OH)_2$ both increases gradually at first and then surges rapidly prior to the second oxidation (Ni^{III}-$Ni^{III/IV}$). When the potential is swept negatively, the conductance decreases with $Ni^{III/IV}$ reduced to Ni^{III}. With the majority of $Ni^{III/IV}$ reduced to Ni^{III}, the sheet conductance drops sharply back to the initial state. The *in situ* conductivity increase/decrease, which reflects the electrical transport characteristics across the surface (intermediate state), is closely related to the $Ni^{III/IV}$ oxidation/reduction. These phenomena are well consistent with the conclusions by previous extended X-ray absorption fine structure (EXAFS) studies[35]. Even more, ETS results show a higher resolution for the different valence states of nickel.

To further establish the relationship between the catalytic performance, resistivity and chemical states of catalysts, a series of doping samples were also tested (Figure 9). The *in situ* electrical conductivity of the γ

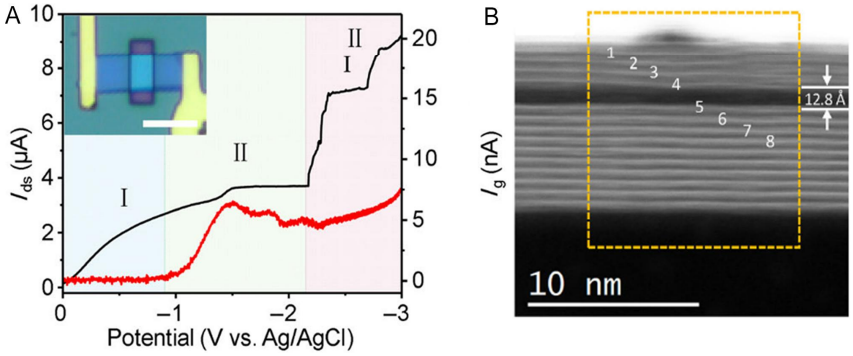

Figure 7 (A) The on-chip *in situ* monitoring of the electrochemical intercalation of PTCDA, with electrochemical (red) and concurrent electrical transport (black) measurements. Inset depicts the optical microscopic image of the device, scale bar is 5 μm. (B) Cross-section STEM-HAADF image of a MoS_2 device after PTCDA intercalation. Reproduced with permission[32]. Copyright 2020, Springer. (color on line)

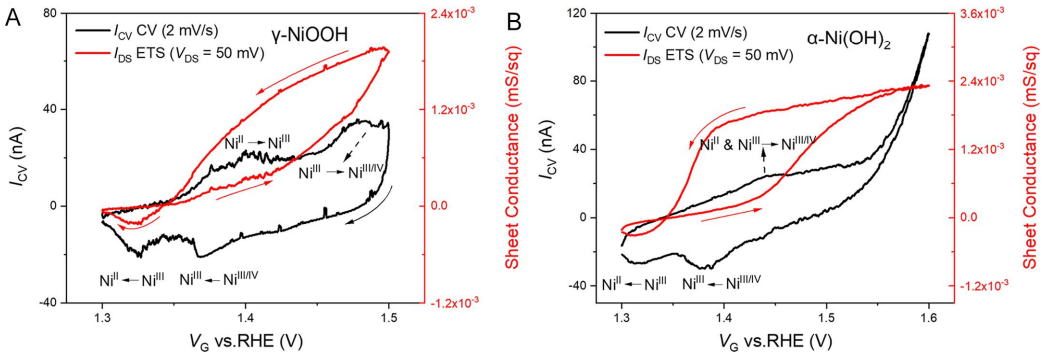

Figure 8 I_{CV}-V_G (CV, black) and I_{DS}-V_G (ETS, red) curves of γ-NiOOH (A) and α-$Ni(OH)_2$ (B) in O_2-saturated 1 mol·L^{-1} KOH. Reproduced with permission[34]. Copyright 2021, John Wiley and Sons. (color on line)

phase intermediates is generally much higher than that of the β phase, which is partly associated with the Ni^{III}-$Ni^{III/IV}$ catalytic active sites and intermediate states with unique electronic structures, while this OER related phase transition does not occur in the β phase. The OER activities from metal doped NiOOH (in both γ and β phases) demonstrate a clear positive correlation to their *in situ* intermediate conductivities. In addition, the potential for the dramatic conductivity increase exactly matches the potential for the second oxidation peak (Ni^{III}-$Ni^{III/IV}$ oxidation). Since the average oxidation state of metal sites during the OER process is highly dependent on the second oxidation level, this observation confirms that the more conductive intermediate surface results from the high-oxidation-state related O containing species that leads to improved OER activity. DFT calculations was further used to characterize the partial density of state (pDOS) of the key OER intermediates[34]. With the formation of M^{IV}-$O^{\cdot}$ for γ-NiOOH with doping by different elements, the contributions from each element were clearly separated. The total charge carrier density (at room temperature) can be further linked to the overall metallic conductivity, and Ni, O and alloying elements all play a distinct role in electrical conductivity. It is known that electron transfer can proceed through oxygen p-orbitals between adjacent metal ions with different d-orbital occupancies, leading to conductive pathways through the double exchange (DE) interaction[36], which is generally used to explain the giant magnetoresistance and metallic behavior of manganese perovskite oxides. Therefore, the DE-induced transport indicator can potentially help elucidate the OER mechanisms in various classes

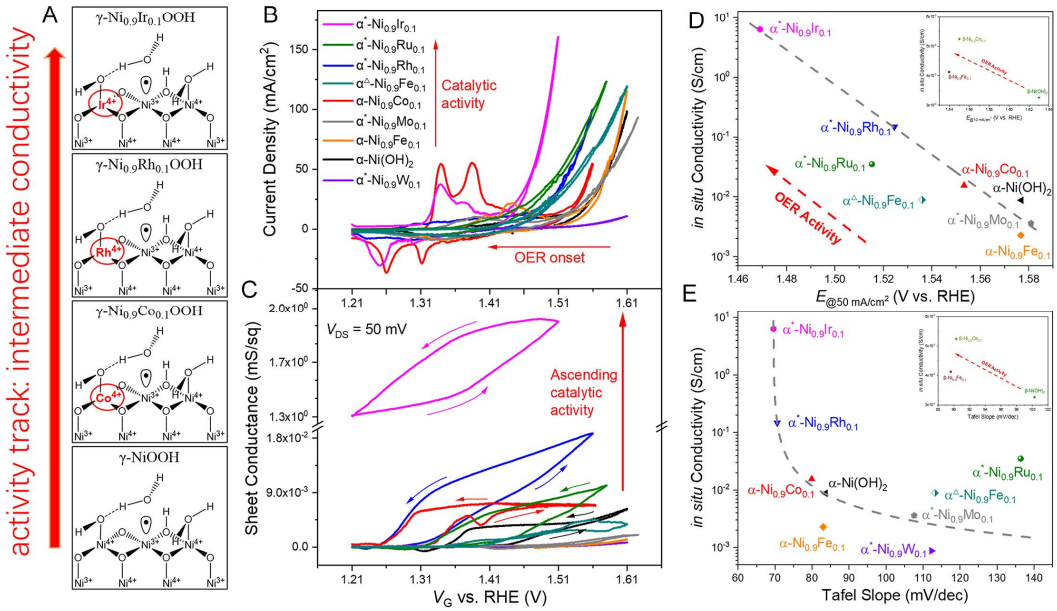

Figure 9 Summary of CV and ETS results for γ and β phases NiOOH for various dopants. (A) The expected structures and oxidation states of γ phase intermediates. (B) The OER catalytic performance (CV) of α phase samples. (C) Corresponding *in situ* sheet conductance (ETS) of the various electrocatalysts in (B). "α^{*}" in (B) denotes pre-oxidation with CV cycles to achieve α-hydroxide formation on the surface. "$\alpha^{\triangle}$" denotes α-$Ni_{0.9}Fe_{0.1}$ sample prepared through ion-exchange. (D) Summary of *in situ* conductivity and OER activity of α and β (inset) phases $Ni_{0.9}M_{0.1}OOH$. (E) Summary of *in situ* conductivity and Tafel slopes of α and β (inset) phases $Ni_{0.9}M_{0.1}OOH$. Reproduced with permission[34]. Copyright 2021, John Wiley and Sons. (color on line)

of inorganic materials, where the mixed valence metal oxyhydroxide plays an essential role in the electro-oxidative process. Hence, on electrodes modified by different elements, the phase change processes of nickel based oxyhydroxides induce different surface states and electrical transport properties, finally resulting in different OER activities. The involved electrical transport mechanism (double exchange) thus provides a descriptor for the design of catalysts and activity prediction of OER performance.

4.3 Phase Change of Monolayer Bi_2WO_6 during Electrochemical CO_2 Reduction

Electrochemical CO_2 reduction (CO_2RR) serves as an important approach to convert greenhouse gas CO_2 into valuable chemicals and fuels (CO, HCOOH, CH_3OH, C_2H_5OH, CH_4, etc.)[37]. Bismuth (Bi) based materials were of particular interest to yield formic acid with a high faradic efficiency (FE) and large current densities (j), and Bi exposure serves as a basis for satisfying performance. However, the catalysts with high Bi exposure for cathodic conversion of CO_2 to formic acid have been limited to the metallic nanosheets ("bismuthene") and metal-organic frameworks (MOFs)[38-40], posing challenges in material synthesis and catalyst stability at large current densities. In addition, the fundamental basis for the catalytic activity of nonmetallic Bi (such as bismuth oxides) remains unclear.

Liu et al. monitored the conversion of Bi_2WO_6 into a metallic intermediate state by ETS during CO_2RR, and the new and presumably surface metallic phase serves as the active sites leading to high faradaic effi ciency (> 97%) and current density (250 mA·cm^{-2}) for formic acid production[41]. As shown in Figure 10(A), on-chip CV curve clearly shows the electrochemical currents of HER, CO_2RR and oxidation/reduction of Bi_2WO_6. With the potential being swept negatively, the electrical conductance of Bi_2WO_6 shows an immediate and significant increase starting at ~0.0 V (vs. RHE), corresponding to a reduction peak (Bi^{3+} to Bi^{0}) in CV. When the potential positively scans to ~0.5 V vs. RHE, the conductance returns to the initial

low stage. The conductance is increased by two orders of magnitude, which is, therefore, less likely to be caused by the surface adsorption of intermediate species as that on pure metals. Instead, monolayer Bi_2WO_6 presumably undergoes a phase transition to reach an "intermediate" metallic state during the electrocatalytic process (Figure 10(B), (C)). *In situ* electrochemical impedance spectroscopy (EIS) was employed at different applied potentials to provide complementary insights into the catalytic mechanism. Three stages can be clearly identified in R_{ct} (the charge transfer resistance) corresponding to varying electro-kinetics at different potentials. Specially, the change in R_{ct} at 0.1 to -0.1 V matches well a phase change (formation of intermediate surface metallic Bi layer) process[41-43]. *In situ* Raman investigations were also employed to confirm the surface structure change of Bi_2WO_6[41]. The peak intensities of Bi-O and O-W-O in monolayer Bi_2WO_6 were gradually reduced starting from -0.1 V vs. RHE. At higher overpotentials, these peaks completely disappear, and peaks for Bi (0) were observed. The metallic intermediate state was also detected by XRD[41]. Post-electrolysis XRD further indicates the final formation of $Bi_2O_2CO_3$, presumably through the formation of metallic intermediates, the loss of the intermediate layer $[WO_4]^{2-}$ ions and the post-electrolysis reaction with carbonate in the electrolyte. Therefore, while monolayer Bi_2WO_6 shows highly efficient CO_2RR, ETS was used for the sensitive detection of metallic intermediates during the catalytic process. This work is also a good example that multiple *in situ* technologies including *in situ* EIS, *in situ* Raman and XRD provide complement information concerning the electro-kinetics, surface adsorptions, and evolution of the catalyst structures.

4.4 Self-Gating in Semiconductor Electrocatalysis

While the semiconductor-electrolyte interface,

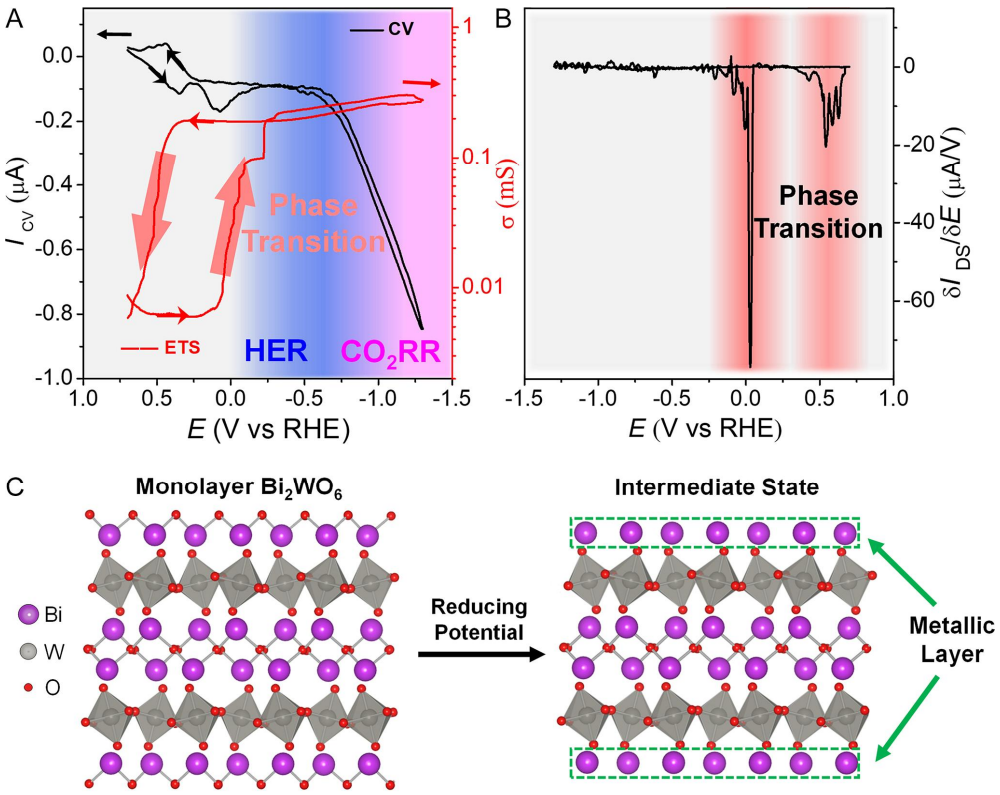

Figure 10 (A) Typical CV (black) and ETS (red) curves of the monolayer Bi_2WO_6 device in 0.5 mol·L^{-1} CO_2-saturated $KHCO_3$. (B) dETS result of (A). (C) Schematic illustration of the surface phase transition in monolayer Bi_2WO_6 with reducing potentials. Reproduced with permission[41]. Copyright 2021, American Chemical Society. (color on line)

which dominants semiconductor electrocatalytic performances, has attracted much attention, the electron transfer between semiconductor and electrolyte and the key factors remain under debate owing to the difficulty in identifying the surface (physical/chemical) states of electrodes[44-46]. He et al. monitored the conductivity change of 2D semiconductors (p-type, n-type, bipolar-type) by ETS measurements under electrochemical conditions, proposing self-gating mechanism[47]. As shown in Figure 11(A), with the negative potential scanning, the drain-source current I_{SD} of WS_2 shows an on/off ratio of 104. The obvious conductance modulation is usually observed on a classic field-effect transistor (FET), which however can also be achieved without any additional gate electrode in electrochemical processes. Therefore, this phenomenon is termed self-gating. It is remarkable that WS_2 was turned on with a potential earlier than that of HER, indicating a possible connection between conductance and HER performance. In order to further confirm and clarify the above conclusions, *in situ* EIS was performed to reveal the reduced internal resistance of MoS_2 during electrocatalysis[47]. The results of MoS_2 with different thicknesses show that the penetration depth of the surface conductance is lower than 40 nm. For catalysts with thinner thickness, electrons are more likely to be transferred from substrate to the highly conductive surface (Figure 11(B)), that is, the electrocatalytic reaction take s place, which further results in higher electrocatalytic activity. This effect can be used to explain the thickness-dependent electrocatalytic activity. Based on the above research, the "self-gating" phenomenon can be extended to complete semiconductor systems, thus establishing the relationship between the type of semiconductor materials and electrocatalytic performances (Figure 11(C)-(E)).

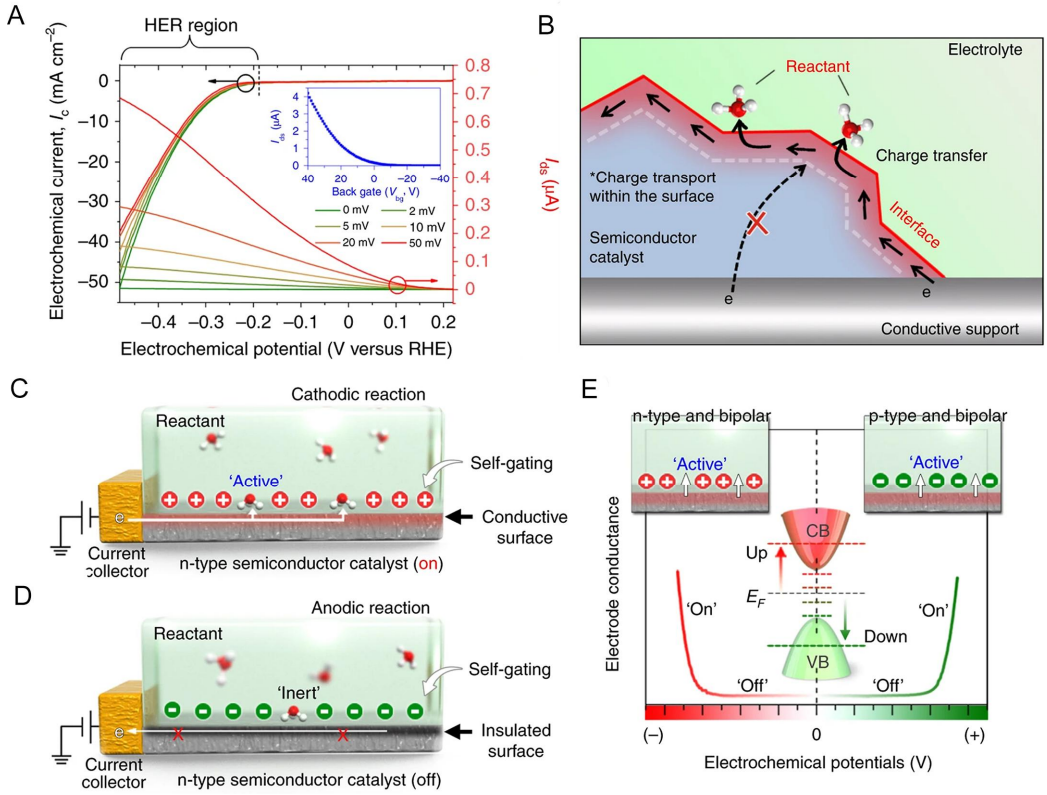

Figure 11 (A) Typical electrochemical (*y* axis in black) and electronic (*y* axis in red) signals of single-layer WS_2 during HER at different bias potentials. (B) Schematic of the surface conductance of the semiconductor electrocatalyst. (C and D) Schematic of the effect of surface conductance on an n-type semiconductor catalyst for a cathodic reaction (C) and an anodic reaction (D). (E) Schematic of the correlation between the types of semiconductor and their preferred electrocatalytic activities. Reproduced with permission[47]. Copyright 2019, Nature Publishing Group. (color on line)

N-type semiconductor catalysts can be turned on by a negative electrochemical potential (positive gating), making them suitable for cathodic reactions, such as HER and CO_2RR. Inversely, p-type semiconductor catalysts can be turned on by a positive electrochemical potential (negative gating), resulting in anodic reactions, such as OER and ORR. Bipolar semiconductor catalysts can be turned on by both positive and negative potentials, leading to anodic and cathodic reactions, respectively. Therefore, ETS was used to monitoring the conductivity change caused by self-gating during active surface reactions, which will allow electrons to be transferred efficiently from the substrate to the outmost surface of electrode materials, leading to higher electrocatalytic performances.

5 Conductive Mechanisms of the Electrochemically Active Cells

Dissimilatory metal-reducing bacteria, such as Shewanella and Geobacter spp., can harness energy through the metabolic oxidation of electron donors (organic sources or fuels) and then transfer electron to electron acceptors (minerals)[48]. The electron transfer from cells to the outside solid-state minerals or electrodes is known as extracellular electron transport (EET), which plays an important role in global biogeochemical cycles[49], and serves as the working principle for microbial fuel cell technologies and microbial biofuel productions[50]. However, the EET mechanism has been controversial and concerned for a long time. One hypothesis suggests that electron conduction is based on the electron hopping between adjacent cofactors in the form of a series of redox reactions, while another hypothesis posits a metallic-like conductivity of Geobacter biofilms. It is therefore urgent to provide new experimental evidence about the charge transport mechanisms of long-range electron transport in electrogenic microbial systems.

Ding et al. achieved the direct and concurrent measurements of the electrochemical (I_g) and electrical transport (I_{SD}) currents of *S.* oneidensis MR-1 under physiological conditions through ETS, and found that the electron transport within MR-1 is closely correlated to electrochemical processes[51]. By applying different V_G, the "conductivity" of Shewanella was found positively correlated with the degree of metabolism (Figure 12(A)). Even so, this cannot prove that electron conduction is generated through redox reactions or metal-like conductivity of cells. In order to further clarify the conduction mechanism, the I_{SD}-V_{SD} characteristics of Shewanella and Geobacter were tested using electrode pairs with varying gaps and areas (Figure 12(C), (D))[51]. The electrochemical current should be proportional to the electrode surface area, while the electric transport current should be inversely proportional to the electrode gaps. Experimental electrical transport results show that the electrical transport signal is only significantly affected by the electrode area (Figure 12(D)), confirming that electron conduction is mainly generated through redox reactions, and electron conduction similar to metal is difficult to be achieved directly (Figure 12(B)). This conclusion provides direct evidence of electrical transport mechanisms of cells, and improves the understanding and use of such microbial communities.

6 Conclusions and Future Perspectives

In summary, *in situ* characterization has always been the key for the fundamental and in-depth understanding of electrochemical interfaces and the optimization of electrochemical systems. Electrical transport spectroscopy (ETS), as a new measurement technique with different working principles from traditional *in situ* spectroscopic characterizations, provides unique and effective new information/insights. In this tutorial review, ETS is first introduced for the *in situ* detection and quantitative characterization of redox intermediates and ions on PtNWs, providing guidance for the electrocatalytic processes concerning several typical energy molecules, such as hydrogen peroxide, methanol, formic acid and oxygen gas. Based on the same experimental setup, ETS can be extended to study PtNPs and AuNPs, indicating a robust measurement technique that is suitable towards the investigation of broad range of nanocrystalline materials/catalysts. The distinct ionic adsorption features on gold were clearly revealed, particularly for

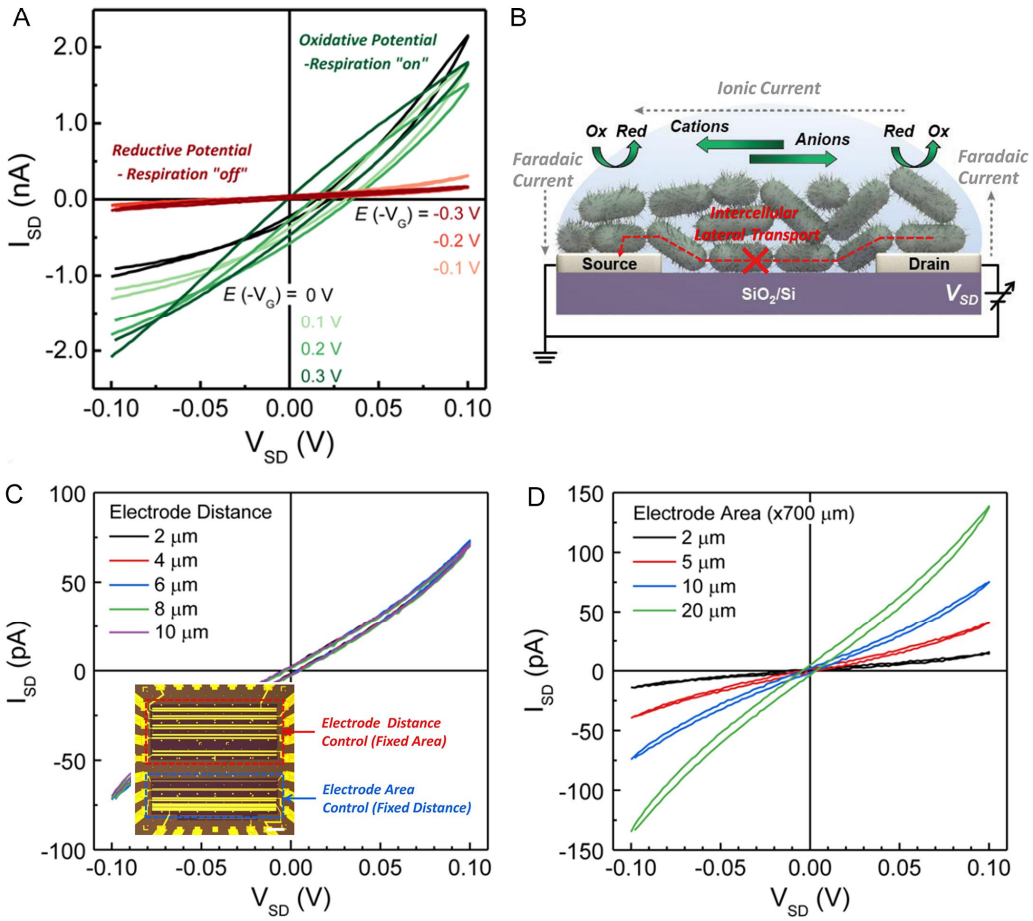

Figure 12 (A) Representative I_{SD}-V_{SD} curves of living MR-1 at different gate voltages. (B) Schematic illustration of the interface electrochemistry model for the electrical conducting current in a typical electrode pair measurement. The transport current is determined by the vertical electron transfer (electrochemical/faradaic current) at the bacteria/electrode interfaces, whereas lateral (non-faradaic) electron transport pathway across the biofilm does not exist. Ionic transport (current) toward the electrodes in the lateral direction forms a complete electrochemical circuit. (C and D) I_{SD}-V_{SD} curves of living Shewanella biofilms with different pair electrode distances (C) and different electrode areas (D). Inset in (C) shows schematic illustration of the biofilm measurements using two sets of pair electrodes with either varying gaps (with fixed areas) or varying electrode areas (with fixed gaps). Reproduced with permission[51]. Copyright 2016, American Chemical Society. (color on line)

the sensitive characterization of perchlorate adsorption (weak adsorbates). Although ETS was originally developed for metallic materials based on the working principle of surface electron scattering, the experimental method matches variation of electrical transport signal in different material systems during active electrochemical processes. Hence, ETS has also been used for the detection of phase change and self-gating in nonmetallic materials, such as two-dimensional materials and nickel based oxyhydroxide, providing the basis for material functionalization and the under standing of electrocatalytic mechanism. ETS has even been extended to bio-electrochemical system for investigating the conductive mechanism of Shewanella and Geobacter.

In general, ETS possesses unique advantages such as low requirements of instrumentation, high sensitivity and accuracy of electrical signals, *in situ* and surface-specific signals, miniaturized sampling, applicability for complex electrocatalytic environments, and a wide range of electrode materials and applications. Although great ad vances of ETS have been made in probing electrochemical interfaces, some challenges are yet to be addressed in both fundamental

studies and practical applications:

(1) *Extension of ETS to more metallic materials.* From the recent studies of Pt and Au, ETS has been demonstrated for the sensitive characterizations of reaction intermediates and ion adsorptions on different metallic surfaces. Owing to the unique electronic and lattice structures, each metal shows its distinct surface adsorption features and advantageous direction of applications. Hence, the potential of ETS will be extensively exploited if ETS measurements can be achieved stably on more metal surfaces based on the successful fabrication of devices. This task may be more challenging in non-noble metal systems, such as copper-catalyzed carbon dioxide reduction[52]. In addition, some metals (Cu, Ni, Bi and et al.) can be easily oxidized in air atmosphere, which presents additional difficulties in fabricating devices with excellent electrical transport property. Even if integrated onto the chip, the metals may undergo severe electrochemical dissolution during oxide formation/reduction processes, posing negative effects on the stability of the testing devices. Therefore, fabricating new devices of metallic materials and ensure stable measurements (may require the advancement of new device structure) is crucial to the future development of ETS.

(2) *Extension of ETS to more non-metallic materials*. Similar to metals, non-metallic materials are characterized based on the successful fabrication of devices. Specifically, for non-metallic materials, it is more necessary to explore the conductive mechanisms and the corresponding application directions. Taking the electrochemical intercalation introduced in this paper as an example, the intercalation process may dramatically change the conductivity of two-dimensional layered materials, which can be associated with a phase change process, and in turn, the phase change will lead to the optimization of the potential range for intercalation. Therefore, non-metallic materials with different conductive mechanisms and applications are yet to be extensively explored.

(3) *ETS measurements of single-entity*. With the on-going development of electrochemistry, it is usually desired to obtain more accurate chemical/physical information of materials with collective and statistic quantification of a considerable number of single entities, thus deriving the research fields of single particle, single molecule, single cell, et al[53-56]. Hence, the future development of ETS can be focused on the measurement of single-material, which may require the special design of devices and electrochemical cells.

(4) *ETS measurements of biological samples*. The measurement and study of living system are extremely challenging due to their structural and compositional complexity, such as proteins, nucleic acids, small molecules, virus, cells, and etc. As mentioned above, ETS measurements have been successfully conducted for the study of conduction mechanism and electrochemical activity of metal-reducing bacteria. For other energy conversion microorganisms such as Sporomusa ovata, which can accept electrons for the reduction of carbon dioxide to acetate[57-58], the involved electrical transport characterizations can be potentially obtained through ETS. In addition, the sensing of biomolecules, cells and viruses have long depended on conductive devices[59-64]. The regulation of vascular permeability and cell membrane ion channels, detection of trace amounts of biological molecules in single-cell rely on the adding of electrical stimulation or electrochemical potential[65-66]. The maximum advantage of ETS technique lies in the combination of electrochemical and electrical measurements within a unique on-chip platform that is also compatible to the CMOS technologies. Hence, ETS theoretically matches these electrical/electrochemical detections and processes, providing a platform for further and in-depth investigation of specific biochemical systems.

(5) *Coupling ETS with other in situ characterization techniques*. The identification of electrical transport signals is crucial to study metallic materials, non-metallic materials and biological species. ETS signals of the metals mainly originate from electron scattering, which may be hard to understand in some cases due to the lack of chemical structure information of adsorbates, and it is approximately the same for non-metallic materials and biological species.

Thus, the identification of ETS signals could be complemented by other *in situ* electrochemical information, such as *in situ* EIS and *in situ* electrochemical spectroscopy. The electrochemical investigations rely on the multi-level support of various characterization methods and signals to promote the development of the whole electrochemical field.

Acknowledgements:

We acknowledge the support by the Natural Science Foundation of China (22172075), the Fundamental Research Funds for the Central Universities in China (0210/14380174), and the "Innovation and Entrepreneurship" program and Jiangsu Province.

References:

[1] Motobayashi K, Osawa M. Recent advances in spectroscopic investigations on ionic liquid/electrode interfaces [J]. Curr. Opin. Electrochem., 2018, 8: 147-155.

[2] Zhu Y P, Wang J L, Chu H, Chu Y C, Chen H M. *In situ*/*operando* studies for designing next-generation electrocatalysts[J]. ACS Energy Lett., 2020, 5(4): 1281-1291.

[3] Deng Y L, Yeo B S. Characterization of electrocatalytic water splitting and CO_2 reduction reactions using *in situ*/*operando* Raman spectroscopy[J]. ACS Catal., 2017, 7(11): 7873-7889.

[4] Timoshenko J, Cuenya B R. *In situ*/*operando* electrocatalyst characterization by X-ray absorption spectroscopy[J]. Chem. Rev., 2021, 121(2): 882-961.

[5] Yang K L, Kas R, Smith W A. *In situ* infrared spectroscopy reveals persistent alkalinity near electrode surfaces during CO_2 electroreduction[J]. J. Am. Chem. Soc., 2019, 141(40): 15891-15900.

[6] Polcari D, Dauphin-Ducharme P, Mauzeroll J. Scanning electrochemical microscopy: A comprehensive review of experimental parameters from 1989 to 2015[J]. Chem. Rev., 2016, 116(22): 13234-13278.

[7] Hui F, Lanza M. Scanning probe microscopy for advanced nanoelectronics[J]. Nat. Electron., 2019, 2(6): 221-229.

[8] Meddings N, Heinrich M, Overney F, Lee J S, Ruiz V, Napolitano E, Seitz S, Hinds G, Raccichini R, Gabers M, Park J. Application of electrochemical impedance spectroscopy to commercial Li-ion cells: A review[J]. J. Power Sources, 2020, 480: 228742.

[9] Pajkossy T, Jurczakowski R. Electrochemical impedance spectroscopy in interfacial studies[J]. Curr. Opin. Electrochem., 2017, 1(1): 53-58.

[10] Ding M N, He Q Y, Wang G M, Cheng H C, Huang Y, Duan X F. An on-chip electrical transport spectroscopy approach for *in situ* monitoring electrochemical interfaces[J]. Nat. Commun., 2015, 6: 7867.

[11] Ding M N, Liu Y, Wang G M, Zhan Z P, Yin A X, He Q Y, Huang Y, Duan X F. Highly sensitive chemical detection with tunable sensitivity and selectivity from ultrathin platinum nanowires[J]. Small, 2017, 13(5): 1602969.

[12] Yang F, Donavan K C, Kung S C, Penner R M. The surface scattering-based detection of hydrogen in air using a platinum nanowire[J]. Nano Lett., 2012, 12(6): 2924-2930.

[13] Sondheimer E H. The mean free path of electrons in metals[J]. Adv. Phys., 2001, 50(6): 499-537.

[14] Climent V, Feliu J M. Thirty years of platinum single crystal electrochemistry[J]. J. Solid State Electrochem., 2011, 15(7-8): 1297-1315.

[15] Wang P T, Zhang X, Zhang J, Wan S, Guo S J, Lu G, Yao J L, Huang X Q. Precise tuning in platinum-nickel/nickel sulfide interface nanowires for synergistic hydrogen evolution catalysis[J]. Nat. Commun., 2017, 8: 14580.

[16] Reier T, Oezaslan M, Strasser P. Electrocatalytic oxygen evolution reaction (OER) on Ru, Ir, and Pt catalysts: A comparative study of nanoparticles and bulk materials[J]. ACS Catal., 2012, 2(8): 1765-1772.

[17] Fukuzumi S, Yamada Y, Karlin K D. Hydrogen peroxide as a sustainable energy carrier: electrocatalytic production of hydrogen peroxide and the fuel cell[J]. Electrochim. Acta, 2012, 82: 493-511.

[18] Chang X, Batchelor-McAuley C, Compton R G. Hydrogen peroxide reduction on single platinum nanoparticles [J]. Chem. Sci., 2020, 11(17): 4416-4421.

[19] Ali A, Shen P K. Recent advances in graphene-based platinum and palladium electrocatalysts for the methanol oxidation reaction[J]. J. Mater. Chem. A, 2019, 7(39): 22189-22217.

[20] Ferre-Vilaplana A, Perales-Rondón J V, Feliu J M, Herrero E. Understanding the effect of the adatoms in the formic acid oxidation mechanism on Pt(111) electrodes[J]. ACS Catal., 2014, 5(2): 645-654.

[21] Banerjee S, Zhang Z Q, Hall A S, Thoi V S. Surfactant perturbation of cation interactions at the electrode-electrolyte interface in carbon dioxide reduction[J]. ACS Catal., 2020, 10(17): 9907-9914.

[22] Cho M, Song J T, Back S, Jung Y, Oh J. The role of adsorbed CN and Cl on an Au electrode for electrochemical CO_2 reduction[J]. ACS Catal., 2018, 8(2): 1178-1185.

[23] Huang J E, Li F W, Ozden A, Rasouli A S, de Arquer F P G, Liu S J, Zhang S Z, Luo M C, Wang X, Lum Y W, Xu Y, Bertens K, Miao R K, Dinh C T, Sinton D, Sargent E H. CO_2 electrolysis to multicarbon products in strong acid[J]. Science, 2021, 372(6546): 1074-1078.

[24] Dubouis N, Serva A, Berthin R, Jeanmairet G, Porcheron B, Salager E, Salanne M, Grimaud A. Tuning water reduction through controlled nanoconfinement within an organic liquid matrix[J]. Nat. Catal., 2020, 3(8): 656-663.

[25] Ding M, Zhong G Y, Zhao Z P, Huang Z H, Li M F, Shiu H Y, Liu Y, Shakir I, Huang Y, Duan X F. On-chip *in situ* monitoring of competitive interfacial anionic chemisorption as a descriptor for oxygen reduction kinetics[J]. ACS Cent. Sci., 2018, 4(5): 590-599.

[26] Mu Z Y, Yang M, He W, Pan Y H, Zhang P K, Li X F, Wu X J, Ding M N. On-chip electrical transport investigation of metal nanoparticles: Characteristic acidic and alkaline adsorptions revealed on Pt and Au surface[J]. J. Phys. Chem. Lett., 2020, 11(14):5798-5806.

[27] Valter M, Busch M, Wickman B, Grönbeck H, Baltrusaitis J, Hellman A. Electrooxidation of glycerol on gold in acidic medium: A combined experimental and DFT study[J]. J. Phys. Chem. C, 2018, 122(19): 10489-10494.

[28] Liu Y, Weiss N O, Duan X D, Cheng H C, Huang Y, Duan X F. Van der Waals heterostructures and devices[J]. Nat. Rev. Mater., 2016, 1(9): 16042.

[29] Liu Y, Huang Y, Duan X F. Van der Waals integration before and beyond two-dimensional materials[J]. Nature, 2019, 567(7748): 323-333.

[30] He Q Y, Lin Z Y, Ding M N, Yin A X, Halim U, Wang C, Liu Y, Cheng H C, Huang Y, Duan X F. *In situ* probing molecular intercalation in two-dimensional layered semiconductors[J]. Nano Lett., 2019, 19(10), 6819-6826.

[31] Zhang J S, Yang A K, Wu X, van de Groep J, Tang P Z, Liu S R, Liu B F, Shi F F, Wan J Y, Li Q T, Sun Y M, Lu Z Y, Zheng X L, Zhou G M, Wu C L, Zhang S C, Brongersma M L, Li J, Cui Y. Reversible and selective ion intercalation through the top surface of few-layer MoS_2[J]. Nat. Commun., 2018, 9: 5289.

[32] He W, Zang H, Cai S H, Mu Z Y, Liu C, Ding M N, Wang P, Wang X R. Intercalation and hybrid heterostructure integration of two-dimensional atomic crystals with functional organic semiconductor molecules[J]. Nano Res., 2020, 13(11): 2917-2924.

[33] Yu X Y, Feng Y, Guan B Y, Lou X W, Paik U. Carbon coated porous nickel phosphides nanoplates for highly efficient oxygen evolution reaction[J]. Energy Environ. Sci., 2016, 9(4): 1246-1250.

[34] Tian B L, Shin H, Liu S T, Fei M C, Mu Z Y, Liu C, Pan Y H, Sun Y M, Goddard W A, Ding M N. Double exchange induced *in situ* conductivity in nickel based oxyhydroxides: An effective descriptor for electrocatalytic oxygen evolution[J]. Angew.Chem. Int. Ed., 2021, 60(30): 16448-16456.

[35] Bediako D K, Lassalle-Kaiser B, Surendranath Y, Yano J, Yachandra V K, Nocera D G. Structure-activity correlations in a nickel-borate oxygen evolution catalyst[J]. J. Am. Chem. Soc., 2012, 134(15): 6801-6809.

[36] de Gennes P G. Effects of double exchange in magnetic crystals[J]. Phys. Rev., 1960, 118(1): 141-154.

[37] Nitopi S, Bertheussen E, Scott S B, Liu X Y, Engstfeld A K, Horch S, Seger B, Stephens I E L, Chan K, Hahn C, Nørskov J K, Jaramillo T F, Chorkendorff I. Progress and perspectives of electrochemical CO_2 reduction on copper in aqueous electrolyte[J]. Chem. Rev., 2019, 119(12): 7610-7672.

[38] Cao C S, Ma D D, Gu J F, Xie X Y, Zeng G, Li X F, Han S G, Zhu Q L, Wu X T, Xu Q. Metal-organic layers leading to atomically thin bismuthene for efficient carbon dioxide electroreduction to liquid fuel[J]. Angew. Chem. Int. Ed., 2020, 59(35): 15014-15020.

[39] Yang H, Han, N, Deng J, Wu J H, Wang Y, Hu Y P, Ding P, Li Y F, Li Y G, Lu J. Selective CO_2 reduction on 2D mesoporous Bi nanosheets[J]. Adv. Energy Mater., 2018, 8(35): 1801536.

[40] Zhou Y, Liu S T, Gu Y M, Wen G H, Ma J, Zuo J L, Ding M N. In(III) metal-organic framework incorporated with enzyme-mimicking nickel bis(dithiolene) ligand for highly selective CO_2 electroreduction[J]. J. Am. Chem. Soc., 2021, 143(35): 14071-14076.

[41] Liu S T, Wang C, Wu J H, Tian B L, Sun Y M, Lv Y, Mu Z Y, Sun Y X, Li X S, Wang F Y, Wang Y Q, Tang L Y, Wang P, Li Y F, Ding M N. Efficient CO_2 electroreduction with a monolayer Bi_2WO_6 through a metallic intermediate surface state[J]. ACS Catal., 2021, 11(20): 12476-12484.

[42] Chen W, Xie C, Wang Y Y, Zou Y Q, Dong C L, Huang Y C, Xiao Z H, Wei Z X, Du S Q, Chen C, Zhou B, Ma J M, Wang S Y. Activity origins and design principles of nickel-based catalysts for nucleophile electrooxidation[J]. Chem, 2020, 6(11): 2974-2993.

[43] Wang H Y, Hung S F, Chen H Y, Chan T S, Chen H M, Liu B. In operando identification of geometrical-site-dependent water oxidation activity of spinel Co_3O_4[J]. J. Am. Chem. Soc., 2016, 138(1): 36-39.

[44] Gerischer H. Charge transfer processes at semiconductor-electrolyte interfaces in connection with problems of catalysis[J]. Surf. Sci., 1969, 18(1): 97-122.

[45] Bisri S Z, Shimizu S, Nakano M, Iwasa Y. Endeavor of

iontronics: From fundamentals to applications of ion-controlled electronics[J]. Adv. Mater., 2017, 29(25): 1607054.

[46] Marcus R A. On the theory of oxidation-reduction reactions involving electron transfer. I[J]. J. Chem. Phys., 2004, 26(4): 867-871.

[47] He Y M, He Q Y, Wang L Q, Zhu C, Golani P, Handoko A D, Yu X C, Gao C T, Ding M N, Wang X W, Liu F C, Zeng Q S, Yu P, Guo S S, Yakobson B I, Wang L, Seh Z W, Zhang Z H, Wu M H, Wang Q J, Zhang H, Liu Z. Self-gating in semiconductor electrocatalysis[J]. Nat. Mater., 2019, 18(10): 1098-1104.

[48] Nealson K H, Saffarini D. Iron and manganese in anaerobic respiration: Environmental significance, physiology, and regulation[J]. Annu. Rev. Microbiol., 1994, 48: 311-343.

[49] Fredrickson J K, Romine M F, Beliaev A S, Auchtung J M, Driscoll M E, Gardner T S, Nealson K H, Osterman A L, Pinchuk G, Reed J L, Rodionov D A, Rodrigues J L M, Saffarini D A, Serres M H, Spormann A M, Zhulin I B, Tiedje J M. Towards environmental systems biology of Shewanella[J]. Nat. Rev. Microbiol., 2008, 6(8): 592-603.

[50] Rabaey K, Rozendal R A. Microbial electrosynthesis-revisiting the electrical route for microbial production[J]. Nat. Rev. Microbiol., 2010, 8(10): 706-716.

[51] Ding M N, Shiu H Y, Li S L, Lee C K, Wang G M, Wu H, Weiss N O, Young T D, Weiss P S, Wong G C L, Nealson K H, Huang Y, Duan X F. Nanoelectronic investigation reveals the electrochemical basis of electrical conductivity in Shewanella and Geobacter[J]. ACS Nano, 2016, 10(11): 9919-9926.

[52] Gao D F, Soholten F, Cuenya B R. Improved CO_2 elec troreduction performance on plasma-activated Cu catalysts via electrolyte design: Halide effect[J]. ACS Catal., 2017, 7(8): 5112-5120.

[53] Wahab O J, Kang M, Unwi P R. Scanning electrochemical cell microscopy: A natural technique for single entity electrochemistry[J]. Curr. Opin. Electrochem., 2020, 22: 120-128.

[54] Zhang J, Wu J J, Guo H, Chen W B, Yuan J T, Martinez U, Gupta G, Mohite A, Ajayan P M, Lou J. Unveiling active sites for the hydrogen evolution reaction on monolayer MoS_2[J]. Adv. Mater., 2017, 29(42): 1701955.

[55] Inkpen M S, Liu Z F, Li H X, Campos L M, Neaton J B, Venkataraman L. Non-chemisorbed gold-sulfur binding prevails in self-assembled monolayers[J]. Nat. Chem., 2019, 11(4): 351-358.

[56] Gongding J J. Single entity electrochemistry progresses to cell counting[J]. Angew. Chem. Int. Ed., 2016, 55(42): 12956-12958.

[57] Liu C, Gallagher J J, Sakimoto K K, Nichols E M, Chang C J, Chang M C Y, Yang P D. Nanowire-bacteria hybrids for unassisted solar carbon dioxide fixation to value-added chemicals[J]. Nano Lett., 2015, 15(5): 3634-3639.

[58] Nevin K P, Woodard T L, Franks A E, Summers Z M, Lovley D R. Microbial electrosynthesis: feeding microbes electricity to convert carbon dioxide and water to multicarbon extracellular organic compounds[J]. 2010, mBio, 1(2): e00103-10.

[59] Tian B Z, Lieber C M. Nanowired bioelectric interfaces [J]. Chem. Rev., 2019, 119(15): 9136-9152.

[60] Patolsky F, Zheng G F, Lieber C M. Fabrication of silicon nanowire devices for ultrasensitive, label-free, real-time detection of biological and chemical species[J]. Nat. Protoc., 2006, 1(4): 1711-1724.

[61] Tian B Z, Liu J, Dvir T, Jin L H, Tsui J H, Qing Q, Suo Z G, Langer R, Kohane D S, Lieber C M. Macroporous nanowire na noelectronic scaffolds for synthetic tissues [J]. Nat. Mater., 2012, 11(11): 986-994.

[62] Patolsky F, Timko B P, Yu G H, Fang Y, Greytak A B, Zheng G F, Lieber C M. Detection, stimulation, and inhibition of neuronal signals with high-density nanowire transistor arrays[J]. Science, 2006, 313(5790): 1100-1104.

[63] Li T X, Liang Y Q, Li J H, Yu Y, Xiao M M, Ni W, Zhang Z Y, Zhang G J. Carbon nanotube field-effect transistor biosensor for ultrasensitive and label-free detection of breast cancer exosomal miRNA21[J]. Anal. Chem., 2021, 93(46): 15501-15507.

[64] Tian B Z, Cohen-Karni T, Qing Q, Duan X J, Xie P, Lieber C M. Three-dimensional, flexible nanoscale field-effect transistors as localized bioprobes[J]. Science, 2010, 329 (5993): 830-834.

[65] Jenkins E P W, Finch A, Gerigk M, Triantis I F, Watts C, Malliaras G G. Electrotherapies for glioblastoma[J]. Adv. Sci., 2021, 8(18): 2100978.

[66] Yu R J, Ying Y L, Gao R, Long Y T. Confined nanopipette sensing: From single molecules, single nanoparticles, to single cells[J]. Angew. Chem. Int. Ed., 2019, 58(12): 3706-3714.

电输运谱在原位电化学界面测量应用中的最新进展

穆张岩,丁梦宁 *

(化学与化工学院介观化学重点实验室, 南京大学 化学化工学院, 南京 江苏 210023)

摘要: 电化学/电催化技术是实现能源高效转化与储存的重要手段,并已经发展成为一个国际前沿领域。如今日渐深入的电催化研究开始要求更精确且多维度的电化学界面信息,从而指导实现电化学体系的优化,而这往往依赖于一些原位表征方法的发展和应用。电输运谱(electrical transport spectroscopy,ETS)是一种新兴的基于芯片平台的电化学原位表征技术,它可以实现电势扫描条件下电化学信号和电极材料电输运性质的同时获取。本文首先介绍了基于铂纳米线微纳器件的 ETS 信号原理(吸附现象导致的表面电子散射)和器件制作流程、几个典型电催化反应过程中铂表面状态的演变,以及电解质离子竞争吸附对铂催化氧还原反应动力学过程的影响。由于与电化学体系的高度匹配,ETS 可应用于不同结构及金属类型材料体系(金和铂纳米颗粒)。金和铂表现出显著不同的离子吸附现象,尤其是对于弱吸附离子(高氯酸根和硫酸根)。通过电输运谱还可实时监测电化学过程中材料的相变及电子性质的变化。于是,ETS 可被用于监测和实现二维材料电化学可控插层,理解电催化剂在电催化过程中的相变机制以及相变过程如何影响电催化活性,揭示二维半导体催化剂材料电催化过程的自门控效应。此外,ETS 还被应用于生物电化学体系,探索电化学过程中的细胞导电机制。最后,本文对 ETS 的优点及不足进行总结,展望了 ETS 在未来电化学领域所面临的挑战和机遇。

关键词: 电输运谱;微纳电化学器件;原位表征;电化学表界面;表面吸附